Experimental And Numerical Study On Concretefilled Steel Tubular Members Under Lateral Impact Load

Hanan H. Eltobgy, AnwarBadawy, Emad Darwish, Mahmoud Morgan

Abstract :AConcrete-filled steel tube (CFST) structure has been widely used in civil engineering structures as it offers numerous structural benefits.The (CFST) columns' behavior has been investigated intensively against axial and lateral impact loading. However, there is a lack of knowledge on the response of (CFST) columns when filled with different types of concrete. Therefore, to close this gap, experimental and numerical studies were carried out to investigate the performance of CFST members filled with four different types of concrete under the effect of lateral impact load. The concrete types were normal concrete, steel fiber concrete, and propylene fiber concrete all with average cubic strength of Fcu=45 N/mm^2, except the last one was high strength concrete with Fcu=70 N/mm^2. In high-loaded members, the available standard tubes' sizes available in domestic market will not cover the required design size, hence emerged the need to fabricate the required size of pipe by welding. Consequently, the effect of using seam weld pipe instead of seamless pipe on the response of (CFST) under impact load was investigated in this study. Accordingly, eight specimens were tested divided into two groups, four specimens for each. The first group is fabricated from a seam weld pipe and the other group from seamless pipe. The parameters studied were types of concrete and steel pipe.The failure mode and local damages of the specimens were thoroughly investigated. A finite element analysis (FEA) model was then performed to simulate the behavior of (CFST) members against lateral impact loading and validated with the corresponding experimental results. Wide range analyses of the (CFST) columns response against lateral impact loading were then carried out using the validated FE models to examine the deformation and the energy dissipation of each concrete type. The main findings are as follows: (1) The seam weld specimens have an almost equivalent lateral impact resistance as seamless CFST counterparts. (2) The lowest value for the total impact energy and maximum dynamic displacement were recorded for the specimens filled with polypropylene concrete specimens. While the maximum recovery energy was observed for the same specimens. (3) Nearly the same value for the total impact energy and maximum dynamic displacement were recorded for the specimens filled with ordinary concrete and high strength concrete.

Index Terms: Impact load, concrete filled steel tube CFST, Steel fiber concrete, propylene fiber concrete, high strength concrete.

1 INTRODUCTION

THE concrete filled steel tubes (CFSTs) are used increasingly in numerous structural applications, such as bridge piers, offshore structures, seismic-resistant constructions, and high-rise buildings due to their excellent constructional and structural performance[1-3]. CFSTs offer more advantages than the conventional reinforced concrete and structural steel members, namely the high speed of construction work resulting from the omission of formwork and reinforcing bars, low structural costs, and conservation of the environment [4, 5]. CFSTs also offer good damping properties and excellent seismic resistance [6]. Moreover, CFSTs have superior fire resistance quality compared with the ordinary reinforced concrete, that leads to a reduction in fireproof materials usage[7].

During the service lifespan, structures may experience impact loading. For examples, bridge columns could be impacted bya vehicle or boat, high risingbuildings could be attacked byan aircraft, or falling loads due to an accidental explosion [8, 9].The columns of bridge piers and a multi-story building are vital structural members and failure associated with an impact loading may trigger progressive collapse and further disproportionate collapse. Therefore, attention should be given to study and understand the elastic–plastic behavior of a column under high impact loading, especially to CFST columns due to the high bearing capacity they provide. Numerous studies have been conducted on CFST members to study their behavior under both static and cyclic loads. CFST was mentioned in several design codes as discussed in [1]. Experimental studies were conducted to investigate the effect of impact load on specimens filled with normal aggregate concrete steel tube (NACFST) and recycled aggregate (RACFST) [10]. They concluded that the square RACFST specimens have an almost equivalent lateral impact resistance as normal CFST specimens. Bambach et al. [11] studied the concrete filled square steel tube behavior subjected to heavy mass and low velocity impact. They proposed an elastic-plastic theoretical model to predict the maximum capacity for the fixed ends CFST member under impact and static loadings based on a rigid-plastic analysis. Also, the impact response of recycled aggregate concrete infilled steel tube columns was investigated [12]. The results indicated that under impact loading both the RACFST and NACFST specimenshad a similar deformation mode, and the additional confinement of the CFRP reduced the global displacement for both types of specimens. Ai-Zhu. et. 2018 conducted an experimental and numerical study on the Lateral impact response of rectangular hollow and partially concrete-filled steel tubular columns [13]. Results indicate that the partially concrete-filled steel tubular (PCFST) specimens hadsuperiorperformance to the rectangular hollow steel tubular (RHST) specimens. The height of concrete filling had affected the failure mode significantly, especially when the specimens were tested under high-impact energy. The impact direction and energy significantly

- *Associate Professor of Structural Engineering, Civil Engineering Department Faculty of Engineering at Shoubra,Benha University, Email: hanan.altobgy@feng.bu.edu.eg*
- *Professor of Steel Structures and Bridges, Civil Engineering Department, Faculty of Engineering at Shoubra, Benha University, Email: Anwar.Badawy@feng.bu.edu.eg*
- *Lecturer of Structure Engineering, Civil Eng. Department, Faculty of Engineering, Shoubra, Benha University, Cairo, Egypt, Email: emad.darwish@feng.bu.edu.eg*
- *Assistant Lecturer of Structure Engineering, Civil Eng. Department, Faculty of Engineering, Shoubra, Benha University, Cairo, Egypt, Email: mahmoud.morgan@feng.bu.edu.eg*

affected the impact resistance of the specimen.The height of concrete filling had affected the failure mode significantly, especially when the specimens were tested under high-impact energy. The impact direction and energy significantly affected the impact resistance of the specimen. Despite numerous previous studies on the structural behavior of the CFST columns under qausi-static loading, the effect of using seam weld pipe instead of seamless pipe has not been elaborately studied and investigated. Especially, in case of using CFST in high loaded members the available standard sizes do not cover the required design size, hence emerged the need to fabricate the required size of pipe by welding. So far only limited numbers of research have been conducted on the behavior of normal CFST columns under lateral impact loadings. However, the impact behavior of steel tube filled with various types of concrete such as steel fiber concrete, polypropylene fiber concrete or high strength concrete have never been researched. Therefore, in this study we seek to investigate the performance of CFST members filled with different types of concrete under the effect of lateral impact load. This research has triplet purposes; First, to conduct a series of new experimental tests on eight circular CFST members under lateral impact load, to includein the testing parameters include the concrete type, the pipe type, as well as the constraining factor. Second, to study the global deformation, and the time history of the impact forces, as well as the absorption energy for each specimen based on the testing results. Third, to provide a finite element analysis (FEA) model using Abaqus software applications for further study on the CFST members under impact loads.

2 EXPERIMENTAL PROGRAM

2.1 Specimen preparation

The experimental testes were carried out on eight circular CFST members. Specimen's outer sectional diameter (D) was 114 mm and 82 with overall length1500mm and effective length of 1200 mm, where the steel tube wall thickness ts for all specimens was 4mm. The specimen's boundary conditions were fixed from one end and sliding for the other end. Detailed information of each specimen is presented in Table 1. Concrete's mix design along with the properties of fresh concrete are shown in Table 2. The abbreviations, "N.C", "P.F.C", "S.F.C" or "H.S.C" are used to describe each specimen. Concrete types were normal concrete, propylene fiber concrete, steel fiber concrete or high strength concrete. The cubic strength of all filling concrete types was (Fcu=45 N/mm2) except for high strength concrete was (Fcu=70 N/mm2).

The initial impact energy induced for all specimens was 4900 J ± 150 J depending on the total drop hammer mass (m) of 390kg and the initial impact velocity (Vo) of 5.03m/sec. During each test, the measurements of the force-time history and the global displacement were recorded. The total impact energy (W) was calculated based on the area under curve of impact load vs total displacement graph as shown in Fig. 8.

The carrying capacity of CFST specimens was determined based on their mechanical property and the section physical dimension. High speed camera was used to record drop hammer during falling, afterwards this record was used to calculate the initial impact velocity immediately before collision between drop hammer along with the CFST members as shown in Fig. 3 & Fig. 4.

TABLE 1.

SPECIMENS PROPERTIES.

SPEC. ID	Pipe Type	Conc. Type FCU(MPA)	ζ	$t_{d.e}$ (ms)	$P_{K.e}$ (KN)	$P_{s.e}$ (KN)	$U_{mm,\ e}$ (mm)	U_{mr} (mm)	W (J)	$W_{Recovery}$ (J)	Concrete failure
Pipe 114.3*4MM Clear Length =1200MM											
SP(1)	S	N.C. FCU=450	1.75	32.6	237	79	64	56	5056	-261	A + B
SP(2)	W	N.C. FCU=450	1.75	32.8	244	79	62	53	4907	-255	A+B
SP(3)	S	P.F.C Fcu =450	1.75	29.9	214	96	59	48	4801	-364	B
SP(4)	W	P.F.C Fcu =450	1.75	31.9	226	86	58	49	4849	-321	B
SP(5)	S	S.F.C Fcu =450	1.75	32.9	284	84	63	53	5135	-210	A
SP(6)	W	S.F.C Fcu =450	1.75	34.4	265	76	64	55	4978	-199	A
SP(7)	S	H.S.C Fcu=700	1.12	35.3	268	79	65	55	4929	-263	B
SP(8)	W	H.S.C Fcu=700	1.12	33.2	284	82	62	52	5005	-282	B

A: tensile cracks at tension side, B: facture of concrete core.

TABLE 2.

MIX DESIGN AND PROPERTIES OF FRESH CONCRETE.

Type	Cement (kg/m3)	Sand (kg/m3)	Aggregate (kg/m3)	Water (kg/m3)	Admi.Type (ltr)		S .F. (kg/m3)	P.F. (kg/m3)	Silica fume	Slump (mm)	Fcu (MPA)	Ec (N/mm2)
					PC	F						
N.C	460	650	1110	185	0	5.5	-	-	-	150	44.5	29818
P.F.C	460	650	1110	185	0	5.5	-	0.9	-	130	46.1	30349
S.F.C	460	650	1080	185	0	5.5	30	-	-	120	46.8	30579
H.S.C	400	700	1100	165	9.5	0	-	-	40	260	70.5	36532

(P.F.) Polypropylene Fiber, (S.F) Steel Fiber. (PC) polycarboxylate. (F) supper plasticizer

2.2 MATERIAL PROPERTIES

Materials used in this study were mild steel for tube, cement, aggregate, steel fibers, and propylene fiber as shown in Fig. 1. These materials were locally supplied and tested in accordance with the relevant EN and BS standards. Ordinary Portland cement CEM I/42.5N complying with the requirements of British Standard BS EN 197-1 [14] was used in the preparation of the concrete in this study. The coarse aggregate was normal aggregate (NA) in a maximum size of 10 mm, graded according to the

British Standard BS 882 [15] This size was selected in proportion with the specimen's diameter. The fine aggregate used in this investigation was normal silicious sand. The concrete was poured in layers and compacted with vibrator in the steel tube. The mean cube compressive strength of the N.C, PP.C, and SF.C concrete was designed with approximately 45 MPa at 28-day. While, for HS.C was approximately 70 MPa. Fig. 2 shows the concrete mixing, pouring, and curing, as well as the concretes cubes and cylinders used to obtain the cube's compressive strength (Fcu) and elastic modulus (Ec).

A standard tensile coupon test was conducted on three samples from the two types of steel tube with the standard dimensions, (seamless and seam weld tubes). The average values of the yield strength, ultimate strength and the elongation are listed in Table 3. The modulus of elasticity were 200GPa, the modulus of elasticity (Es) for seamless and seem weld were 1.92×105 N/mm2 and 2.01×105 N/mm2, respectively.

TABLE 3.
STEEL MATERIAL PROPERTIES

Tube	Yield Stress σ_y Mpa	Ultimate Stress σ_u Mpa	Elongation %
Seamless	291	415	23
Seam weld	326	460	24

(a) Coarse Aggragate (b) Steel Fiber (c) Polypropylene Fiber

Fig. 1*.The Concrete Mix Materials.*

a) Mixing b) Curing c) Con. Cylinders

Fig. 2*.Concrete mixing & curing, and concrete Celen & Cube to be tasted later.*

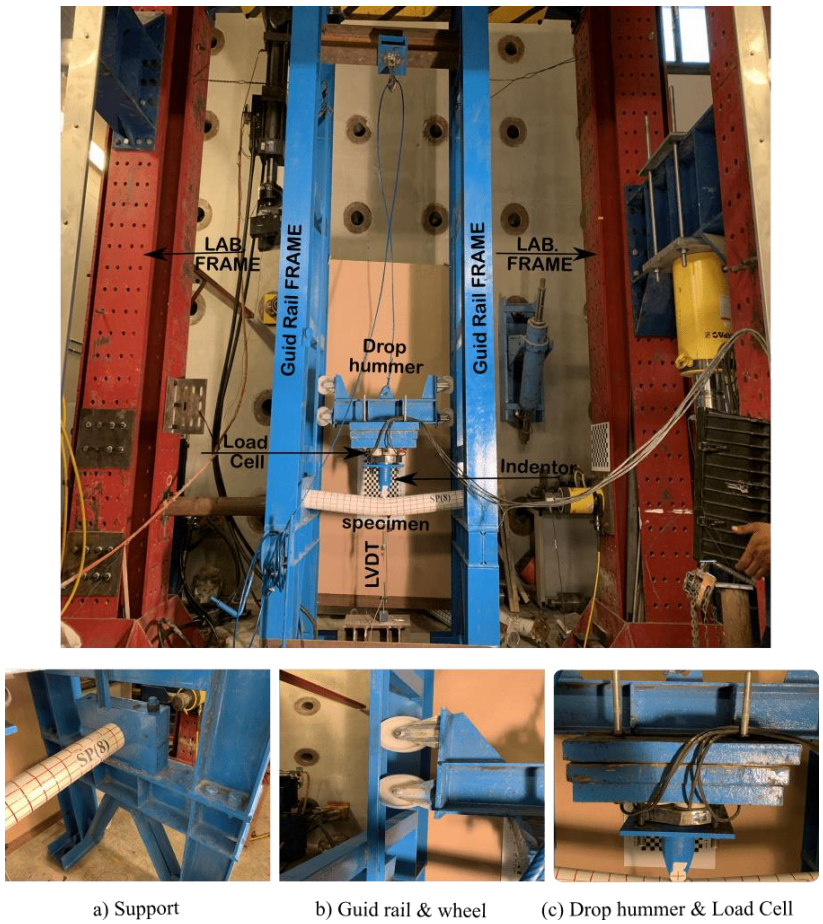

***Fig. 3**. Testing Setting up.*

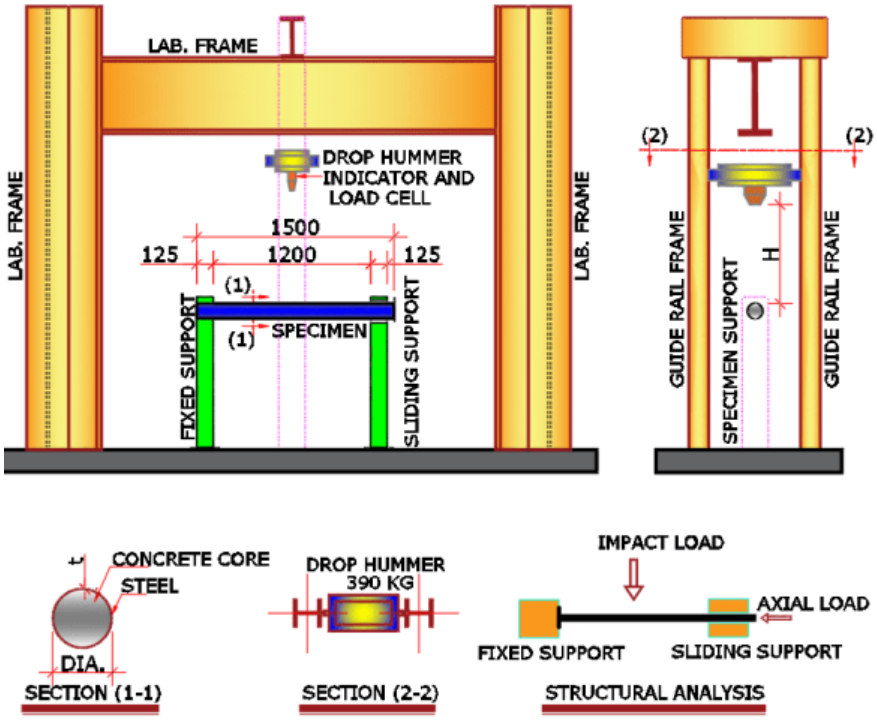

***Fig. 4**. Schematic view for Testing Setting up.*

2.3 TESTING METHOD

The specimens were tested against dynamic lateral impact load, as shown in Fig. 3 & Fig. 4. The specimen was placed in testing device equipped with CFST with fixed-sliding end supports. The mass of the drop hammer was 390 kg, and the impact height (H) was 170 cm. The hammer is formed

from solid steel cylinder with indenter having rigid flat square cross section of 30 mm×80 mm. A load cell was assembled in the drop hummer between the weight and the impactor to record the force–time data during the test. The drop hammer was released from the design height to impose nearly the same impact load at the mid-span of the specimens. The load cell recorded the time-history curves of the impact force and, the time-history curves of displacement were recorded by Linear Voltage Differential Transformer (LVDT).

3 EXPERIMENTAL RESULTS AND DISCUSSIONS

The response of CFST specimens under lateral impact loading was initially represented in a combination of local deformation and global bending, followed by quick increase in the lateral displacement as shown in Fig. 5. The failure started from the initial contact between impact head and the specimens and finished at the same time the impact load basically reached a stable stage. In general, the final the failure pattern of the CFST specimens is characterized by a "V" shape of the specimens within mid-span. The responses of the tested specimens showed a imitative plastic failure mechanism due to bending, and one plastic hinges at the mid-span. The displacement (u) progress of specimen SP (3) is shown in Fig. 6. with 0.042 s interval till reaching the maximum dynamic displacement (umm, e).

The impact load(P) time history of, and the related displacement history applied on the specimen are the most important data recorded during the impact tests. Fig. 7 shows the typical time history of specimen's impact loads. Generally, the impact load (P) versus time (t) history curve pass through three stages, namely oscillation stage (point O to A), stabilization stage (point A to B) and attenuation stage (point B to C) [10]. The stabilization stage (points A and B) is determined based on variation range of P is less than 5 kN within 1 ms. After point A, a sudden change occurred to the slope of P–t curve and started from point B till the end of test. In the oscillation stage, a maximum value of impact load is reached followed by fast decays within a short time. In the stabilization stage the impact load is generally constant. Finally, in the attenuation stage the impact load had been gradually reduced to zero when the impact energy was mostly dissipated. The maximum force recorded in tests is called the experimental peak of impact load (Pk,e) , and the average impact force within the first 15 ms in the stabilization stage is called as the plateau of impact load (Ps,e) as the fluctuation of P small during this period. The time history of impact load (P) for all specimens are shown in Fig. 9. Pk,e and Ps,e are listed in Table 1. The results show that, The least value of Pk.e was recorded for the polypropylene fiber concrete specimens SP(3) & SP(4) with maximum value of 226KN then for normal concrete specimens SP(1) & SP(2) with nearly 8% increase in maximum value of Pk.e to reach 244KN. While, the maximum value for Pk.e was recorded for the steel fiber concrete SP(5) & SP(6), and high strength concrete SP(7) & SP(8) with nearly 25% increase in maximum value of Pk.e to reach 284KN. The plateau value of impact load (Ps,e) for all specimens was ranged between 79 KN and 96 KN. The largest value for the plateau of impact load was recorded for the polypropylene fiber concrete specimens SP(3) & SP(4).

The time histories of mid-span displacement (um) for all specimens are shown in Fig. 9. The maximum dynamic experimental displacement (umm,e) at the mid-span is listed in Table 1. It can be observed that, the polypropylene fiber concrete specimens SP(3) & SP(4) had the least displacement value of 58 &59 mm. While the displacement of other specimens ranged between 62 to 65 mm. The maximum dynamic experimental displacement (umm,e) for the high strength concrete and the ordinary concrete are nearly the same. The concrete strength had no improvement effect on the (umm,e).

The calculation method of the total energy, the absorbed energy, and the recovery energy are illustrated in Fig. 8. The least value of the total energy (W) was recorded for polypropylene fiber concrete specimens SP(3) & SP(4). The normal, and high strength concrete specimens SP(1) & SP(2) & SP(7) & SP(8) had nearly the same total impact energy (W). The largest value of total impact energy (W) was recorded for the steel fiber concrete specimens SP(5) & SP(6). On contrast, the largest value of recovery energy was recorded for polypropylene fiber concrete specimens, then for normal, and high strength concrete specimens, then for the steel fiber concrete specimens.

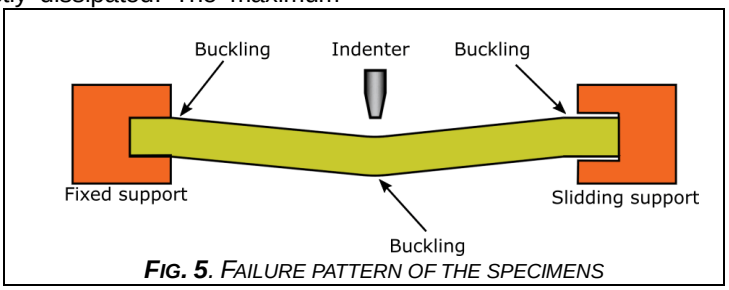

FIG. 5. *FAILURE PATTERN OF THE SPECIMENS*

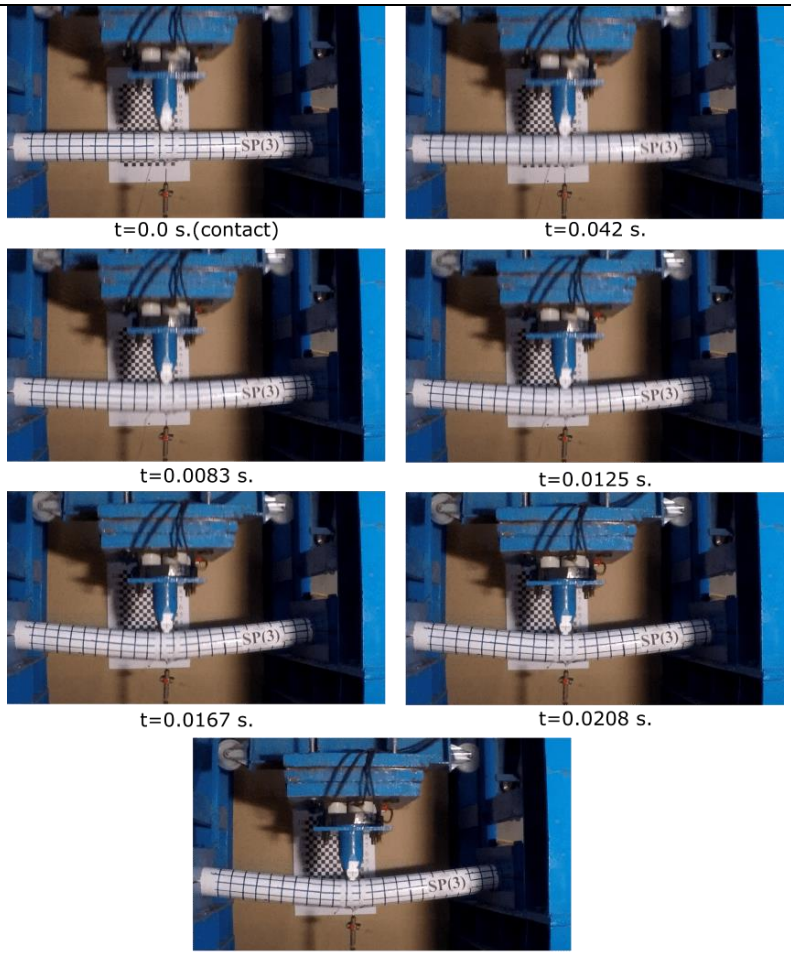

FIG. 6. THE DISPLACEMENT (U) PROGRESS OF SPECIMEN SP(3).

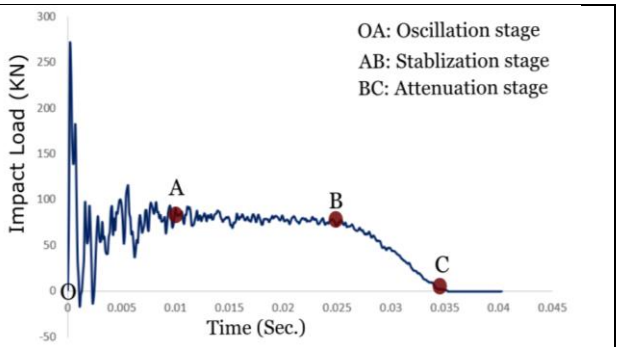

FIG. 7. *TYPICAL TIME HISTORY OF* IMPACT LOADS.

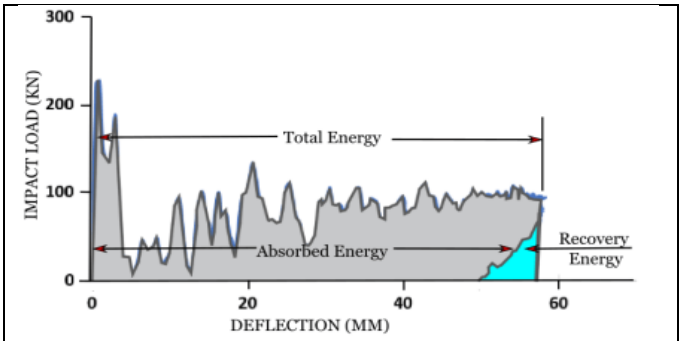

FIG. 8. *THE TOTAL AND ABSORBED ENERGY CALCULATION FOR THE SPECIMENS.*

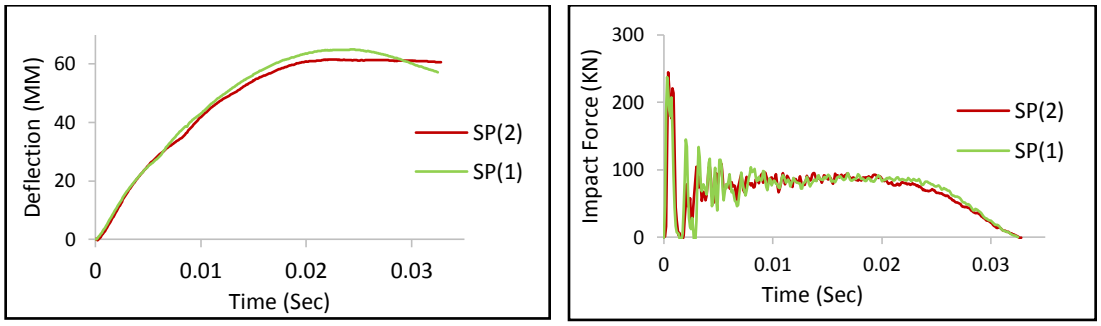

(a) DEFLECTION & IMPACT FORCE VS TIME GRAPH FOR SPECIMENS 1 & 2

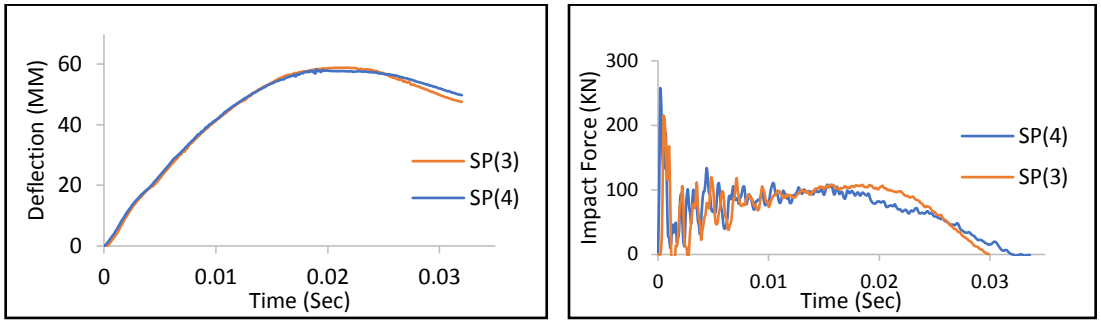

(b) DEFLECTION & IMPACT FORCE VS TIME GRAPH FOR SPECIMENS 3&4

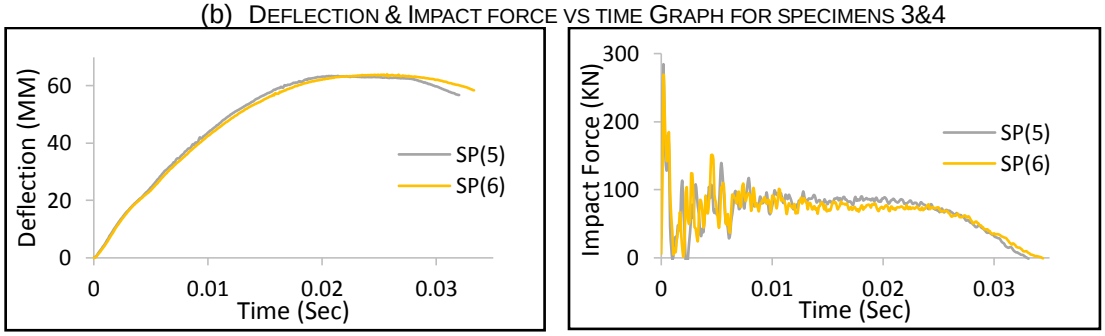

(c) DEFLECTION & IMPACT FORCE VS TIME GRAPH FOR SPECIMENS 5&6

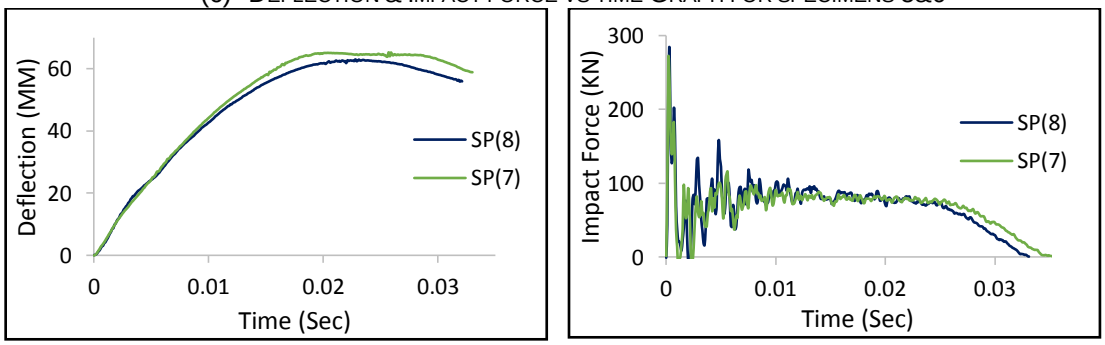

(d) DEFLECTION & IMPACT FORCE VS TIME GRAPH FOR SPECIMENS 7 & 8

***FIG. 9**. DEFLECTION & IMPACT FORCE VS TIME GRAPH FOR ALL SPECIMENS*

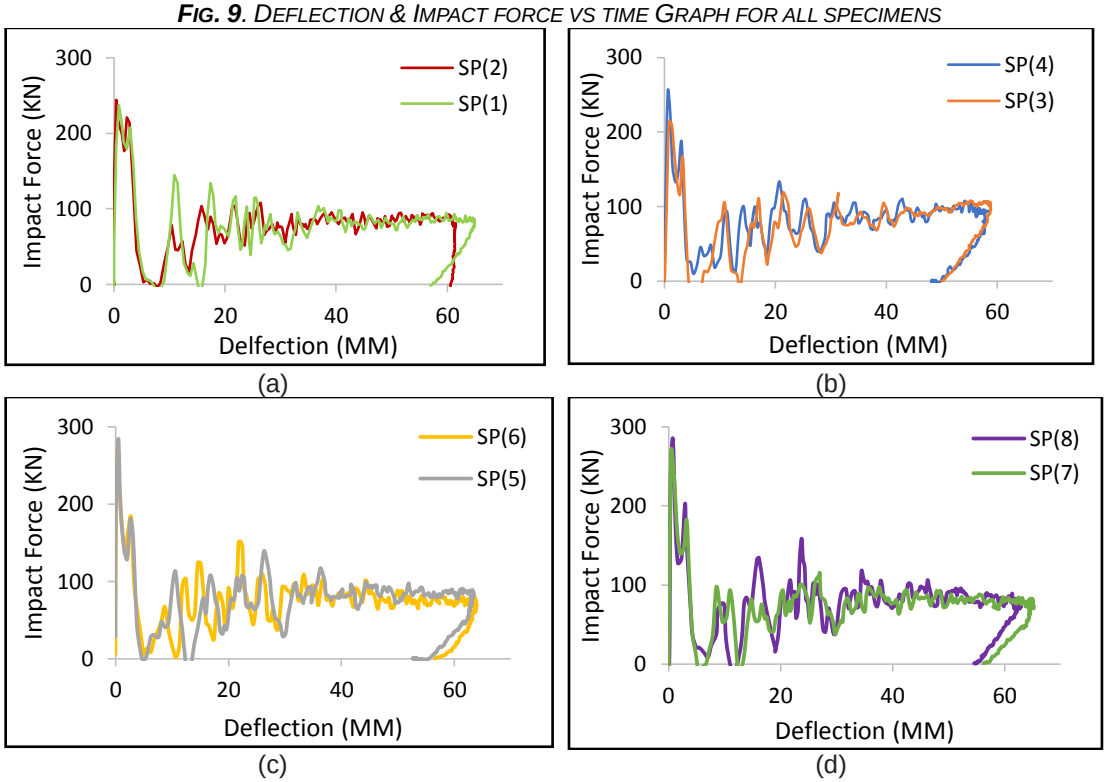

***FIG. 10**. IMPACT FORCE VS DEFLECTION GRAPH FOR ALL SPECIMENS.*

The steel tube buckles on both sides of the impact location. Wide cracks were observed on the concrete core at the tension zone near the impact location for specimens SP(1) & SP(2) of normal concrete. Moreover, a fracture on the concrete core of SP(2) was observed along the flat part between the mid span and the support Fig. 11 (a). while, For specimens SP (7) & SP(8) of high strength concrete, a fracture of the concrete core occurred near the mid span and along the flat part Fig. 11 (d). In specimens SP (3) & SP(4) of polypropylene fiber concrete, a fracture occurred in the concrete core near mid-span without almost any cracks Fig. 11 (b) . In the contrast, in specimens SP (5) & SP(6) of steel fiber concrete, a narrow cracks occurred on the concrete core at the tension zone of the mid-span without any fracture observed Fig. 11 (c).

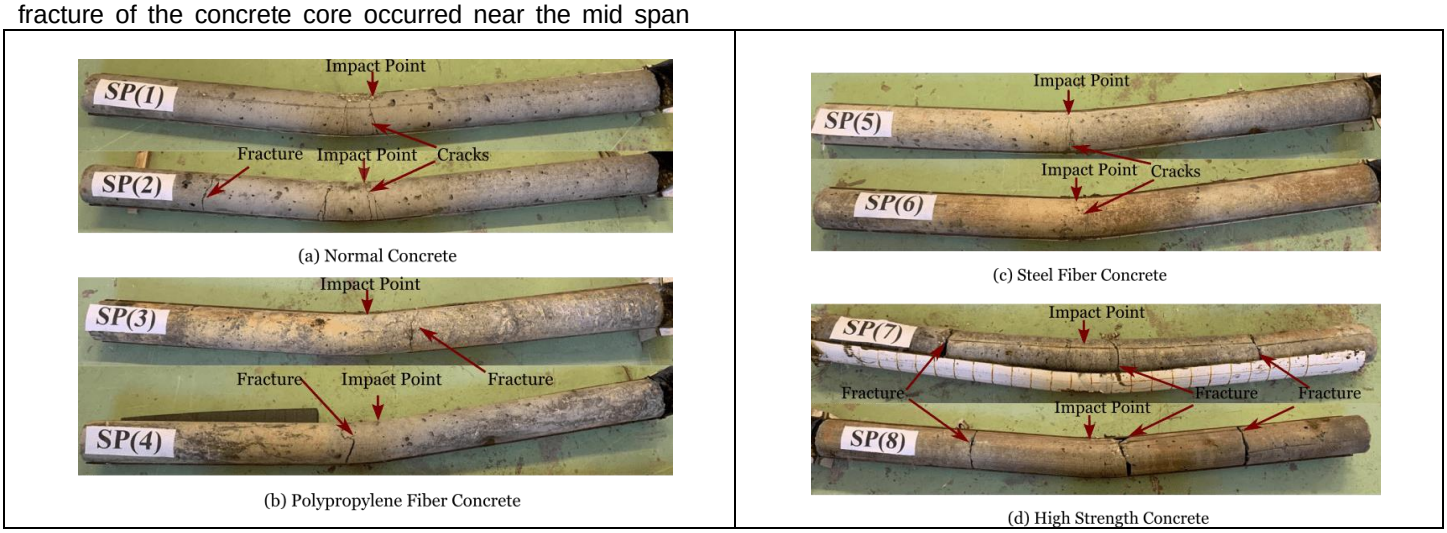

FIG. 11. *FAILURE PATTERN OF THE SPECIMENS.*

4 FINITE ELEMENT ANALYSIS (FEA) MODEL

4.1 DESCRIPTION OF THE FINITE ELEMENT ANALYSIS (FEA) MODEL

A finite element analysis (FEA) model was established using the ABAQUS/Explicit module (Hibbitt et al., 2005 [16]) to understand the performance of CFST elements under lateral impact. To simulate the exact experimental conditions, the components of impact test including the steel tube, the infilling concrete, the interactions between concrete and steel, as well as the hammer, were all simulated in the FEA model. In addition, the boundary conditions, and the element erosion criteria of concrete after impact were considered. The damping forces were not considered due to their insignificant effects during impact and reduction effect on the computational efficiency. The core concrete and the steel tube were modeled by using 8-node brick elements with reduced integration (C3D8R), while the hammer was simplified to a rigid shell surface in the same dimensions (30 x 80 mm) as the contact surface of the indenter especially, it remained almost unchanged during the impact test. The initial impact velocity and mass were assigned to a reference point in the middle surface of the rigid shell to attain the same impact energy during all impact tests. Fig. 2 shows a schematic view of the FEA model of concrete encased CFST member with circular section.

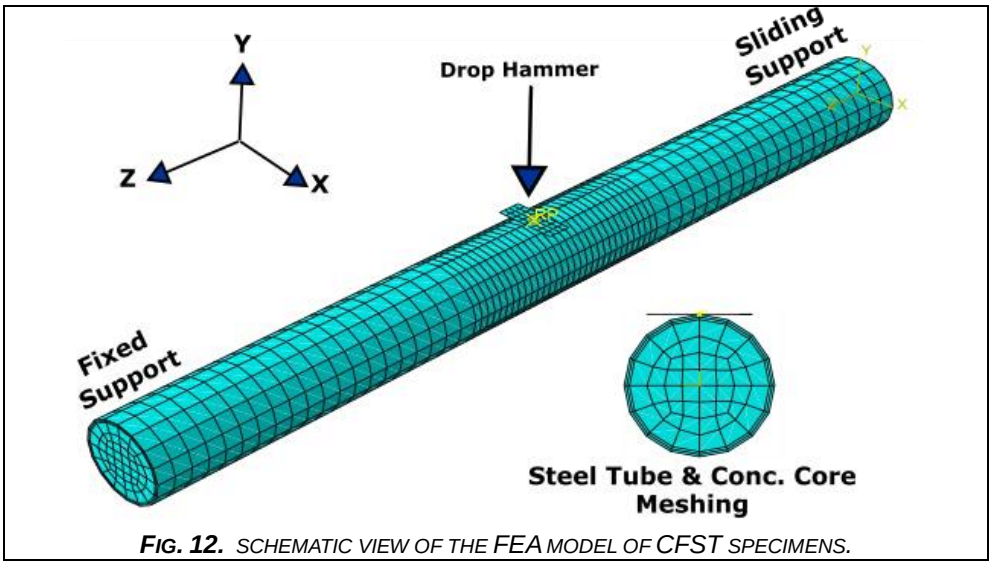

FIG. 12. *SCHEMATIC VIEW OF THE FEA MODEL OF CFST SPECIMENS.*

To ensure the simulating efficiency and achieve reliable results, a mesh convergence study was conducted to identify an appropriate mesh density. Different kinds of element sizes including 5, 10, 15 and 25mm were studied to choose the suitable mesh size for the concrete core and the steel tube. A dense mesh of size 10mm × 25mm was used in the mid-span of the specimen to capture the large deformation, especially the local buckling. Whereas in the other region of specimen a medium mesh density of size of 22 mm × 25 mm was adopted. Stiffness-type hourglasscontrol was considered in the model to eliminate the zero energy modes.

4.2 MATERIALS

4.2.1 Steel

The mild steel material was simulated by using the five-stage stress–strain model proposed by Han et al. (2001)[17] as shown herein .Detailed expressions are given in Pan (1988) as:

$\sigma = E_s \cdot \varepsilon$ for $\varepsilon \le \varepsilon_1$ (1)

$\sigma = -A \cdot \varepsilon^2 + B \cdot \varepsilon + C$ for $\varepsilon_1 \le \varepsilon \le 1.5\varepsilon_1$ (2)

$\sigma = f_{sy}$ for $1.5\varepsilon_1 \le \varepsilon \le 15\varepsilon_1$ (3)

$\sigma = f_{sy} \cdot \left[1 + 0.6 \cdot \frac{\varepsilon - 150\,\varepsilon_1}{135\varepsilon_1}\right]$ for $15\varepsilon_1 \le \varepsilon \le 150\varepsilon_1$ (4)

$\sigma = 1.6 \cdot f_{sy}$ for $\varepsilon > 150\varepsilon_1$ (5)

Where, Es = 200,000MPa, $\varepsilon_1 = 0.8 \cdot f_{sy}$ (the yielding strength of the steel).

The steel modulus of elasticity and Poisson's ratio were assigned based on Table 3. Yield and ultimate strength of steel increase during impact loading with the increase of strain rate [18]. Cowper–Symonds model gives equation to calculate the yield strength of steel under different strain rates as shown in (6.

$$f_y^d / f_y = 1 + (\dot{\varepsilon} / D)^{1/p} \quad (6)$$

f_y is the yield strength of steel tube and f_y^d is the yield strength of steel under strain rate $\dot{\varepsilon}$.The values of D= 6844 s^{-1} andp = 3.91 [19].

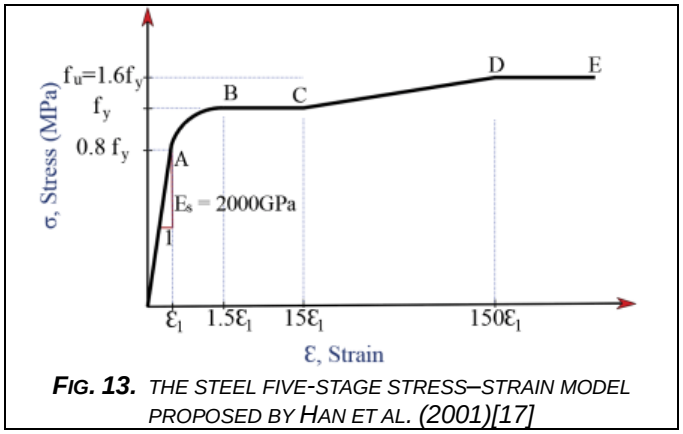

FIG. 13. *THE STEEL FIVE-STAGE STRESS–STRAIN MODEL PROPOSED BY HAN ET AL. (2001)[17]*

The confinement factor ξ was introduced by Han et al. (2001) [17] to quantify the "composite action" of CFST and its expressed as expressed in the following Eq. 7,

$$\xi = \frac{A_S F_y}{A_C F_{ck}} = \alpha \frac{F_y}{F_{ck}} \quad (7)$$

where F_y is the yield strength of steel, F_{ck} is the characteristic concrete strength which equal to 0.67 of the cube strengths of normal concrete, As is the steel tube cross-sectional area, Ac is the concrete core cross-sectional area, and α (=A_s /A_c) is the constraining factor (ξ) was 1.75& 1.12

4.2.2 Concrete

The concrete damaged plasticity model (CDP) in ABAQUS was used to simulate the behavior of core concrete. The following value was adopted for the CDP model, ψ= 30°, e=0.1, f_{b0}/f_{c0} =1.16, and K_c= 2/3 where (ψ) is the dilation angle, (e) is the flow potential eccentricity, (f_{b0}/f_{c0}) is the ratio of the compressive strength under biaxial loading to uniaxial compressive strength, and (K_c) is the ratio of the second stress invariant on the tensile meridian to that on the compressive meridian [20].

In order to simulate the plastic behavior of core concrete in CFSTs under compression, the stress–strain relations presented in Han et al. [21] was later modified by him. [3] based on a large amount of trial calculations on CFST stub column test results to suit for the FEA using ABAQUS software. The modified stress–strain model is represented by (8. The proposed concrete model considered the increase in the plasticity of the concrete core because of the passive confinement of the steel tube as shown in Fig. 14 (a).

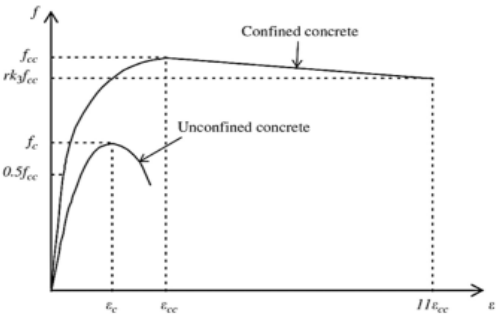

(a) RELATIONSHIP OF CONfiNED AND UNCONfiNED CONCRETE[21]

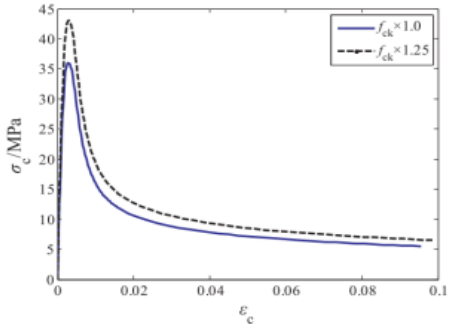

(b) CONCRETE WITH AND WITHOUT DYNAMIC INCREASE FACTOR[13].

FIG. 14. *COMPARISON BETWEEN STRESS-STRAIN CURVES OF CONFINED AND UNCONFINED CONCRETE AND THE EFFECT OF STRAIN RATE ON CONCRETE.*

$$y = \begin{cases} 2x - x^2 & (x \le 1) \\ \dfrac{x}{\beta_0 (x-1)^{\eta} + x} & (x > 1) \end{cases} \quad (8)$$

$$\text{where} x = {}^{\varepsilon}/_{\varepsilon_0}, \quad y = {}^{\sigma}/_{\sigma_o}, \quad \sigma_o = f_c^{'}\left(\frac{N}{mm^2}\right);$$

$$\varepsilon_0 = \varepsilon_c + 800\xi^{0.2} * 10^{-6}; \; \varepsilon_c = (1300 + 12.5\, f_c^{'}) * 10^{-6}$$

$$\eta = \begin{cases} 2 & (\text{CFSTwithcircularsection}) \\ 1.6 + 1.5x & (\text{CFSTwithsquaresection}), \end{cases}$$

$$\beta_0 = \begin{cases} (2.36 * 10^{-5})^{[0.25+(\xi-0.5)^7]} (f_c^{'})^{0.5} * 0.5 \ge 0.12 \\ (\text{CFSTwithcircularsection}) \\ \dfrac{(f_c^{'})^{0.1}}{1.2\sqrt{1+\xi}} \\ (\text{CFSTwithsquaresection}) \end{cases}$$

The strain- curve for the steel fiber concrete are calculated based on the model proposed by Carreira and Chu [22], whose general expression is given by(9,

$$\frac{\sigma_c}{f_c} = \frac{\beta\left({}^{\varepsilon_c}/_{\varepsilon_{c,0}}\right)}{\beta - 1 + \left({}^{\varepsilon_c}/_{\varepsilon_{c,0}}\right)^{\beta}} \quad (9)$$

$$\beta = (0.0536 - 0.5754 V_f) f_c$$

$$\varepsilon_{c,0} = (0.00048 + 0.01886 V_f) \ln f_c$$

where, σ_c is the compressive stress, f_c is the compressive strength, ε_c is the strain, $\varepsilon_{c,0}$ is the peakstrain and β is the factor which considers the influence of fibers on the curve form. The parameters β and$\varepsilon_{c,0}$ can be obtained, in general, by equations that correlates these parameters to fiber volumetric fractionand/or to the compressive strength of concrete. In general, the equations of β and$\varepsilon_{c,0}$ are correlated to fiber volumetric fractionand/or to the compressive strength of concrete [23].

According to the ACI Committee 318 recommendations [24], The initial modulus of elasticity was taken as $Ec = 4730\sqrt{f_c^{'}}$, and Poisson's ration as μc = 0.2, where $f_c^{'}$ was the concrete cylinder strength (in N/mm2), $f_c^{'} = f_{ck} + 8$ [38]. $f_{ck} = 0.67 f_{cu}$ where f_{ck}&f_{cu} are the characteristic static compressive strength, and the average measured cubic compressive strength of concrete at 28 days, respectively. The effect of impact load on the concrete strength was considered by multiplying f_{ck} by a dynamic increase factor of 1.25 [25, 26] as shown in Fig. 14 (b). Moreover, the modulus of elasticity of concrete remained insensitive to the rate of loading [26] .

4.3 Boundary condition and contact

The specimen was fixed from one end while the other end was released only in the longitudinal direction. To demonstrate the contact between the steel tube inner surface and the concrete outer surface, in the normal direction, a surface-based interaction with a contact pressure model “hard contact” was used, thereby allowing the interface separation in tension without penetration of that in compression [33]. A Coulomb friction was used for the model in the tangential direction, thereby the frictional behavior between the surfaces was specified by a friction factor equal to 0.47 according to Baltay et al. [27].

4.4 Verifications of the FEA model

The finite element analysis model was validated by comparing the tested results (including the impact process, the horizontal displacement, and the failure modes) with the predicted results as shown in Fig. 14. The comparison between the measured and the predicted impact force (F) and the displacement vs time (t) curves for the specimens are presented in Figs. 15 &16. The comparisons of impact load (Pk,e), the maximum dynamic experimental displacement (umm,e), and the total impact energy (W) between the experimental and predicted results are demonstrated in Table 4. It can be seen from the figures and table that, the F.E.M can predict well the deformation and impact force of the specimens. A reasonably good agreement between the test and F.E.M results is obtained. However, the total impact energy (W) of the F.E.M are a slightly higher than the tested results. This may contribute to the fact that, the FEA model cannot simulate the friction between devices, effect of air resistance, and environmental interference. Also, the F.E.M did not consider the internal cracks of the steel tube. The unloading trend of the measured impact load history in the test is slower than in the predicted one in the F.E.M. This contributes to the fact that, the expanding of crack in the steel tube would decrease the stiffness of the specimen and thus the trend of the unloading changes.

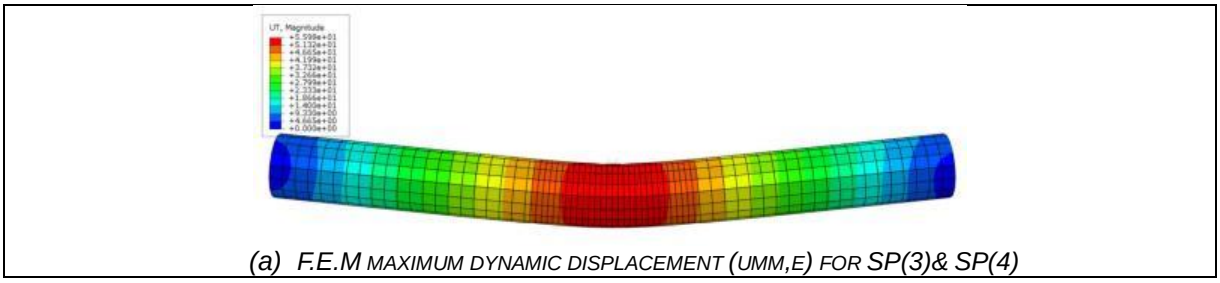

(a) F.E.M MAXIMUM DYNAMIC DISPLACEMENT (UMM,E) FOR SP(3)& SP(4)

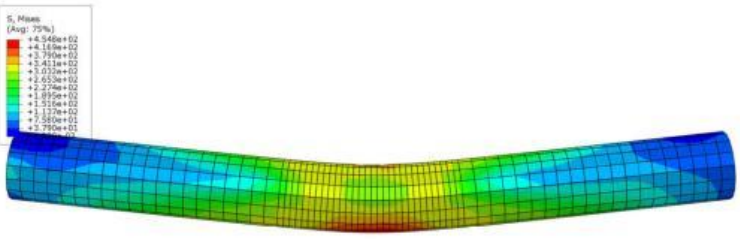

(b) F.E.M VON MISS STRESS OF STEEL TUBE FOR SP(3)& SP(4) CORRESPONDING TO MAXIMUM (UMM,E)

FIG. 15. SAMPLE FOR TYPICAL FAILURE PATTERNS FOR ALL SPECIMENS.

TABLE 4.

INFORMATION OF THE SPECIMENS.

SPEC. ID	Pipe Type	$P_{K.e}$(KN)		F.E.M/ Tested	$U_{mm,e}$ (mm)		F.E.M/ Tested	W (J)		F.E.M/ Tested	Concrete failure
		Tested	F.E.M		Tested	F.E.M		Tested	F.E.M		
Pipe 114.3*4MM Clear Length =1200MM											
SP(1)	S	237	248	1.05	64	63	0.98	5056	5796	1.14	A + B
SP(2)	W	244	248	1.02	62	63	1.02	4907	5796	1.18	A+B
SP(3)	S	214	234	1.09	59	56	0.95	4801	5812	1.21	B
SP(4)	W	226	234	1.04	58	56	0.97	4849	5812	1.20	B
SP(5)	S	284	272	0.96	63	62	0.98	5135	6570	1.28	A
SP(6)	W	265	272	1.03	64	62	0.97	4978	6570	1.32	A
SP(7)	S	268	271	1.01	65	64	0.98	4929	6423	1.30	B
SP(8)	W	284	271	0.95	62	64	1.032	5005	6423	1.28	B

A: tensile cracks at tension side, B: facture of concrete core.

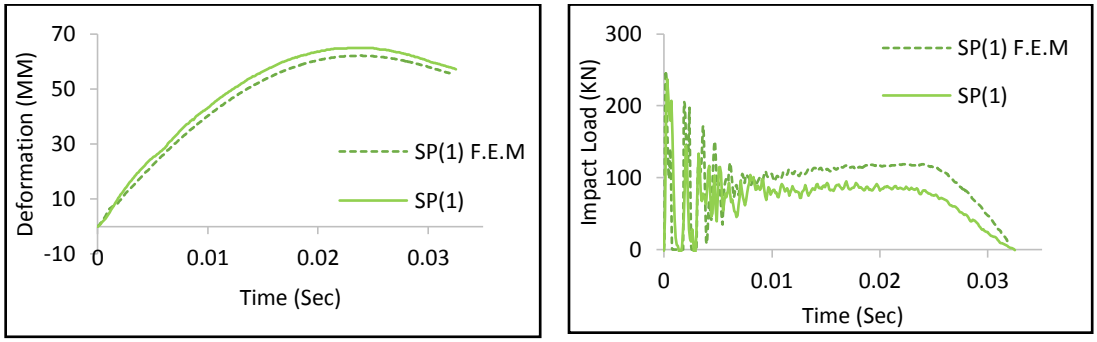

(a) DEFLECTION & IMPACT FORCE VS TIME GRAPH FOR SPECIMEN'S SP(1)

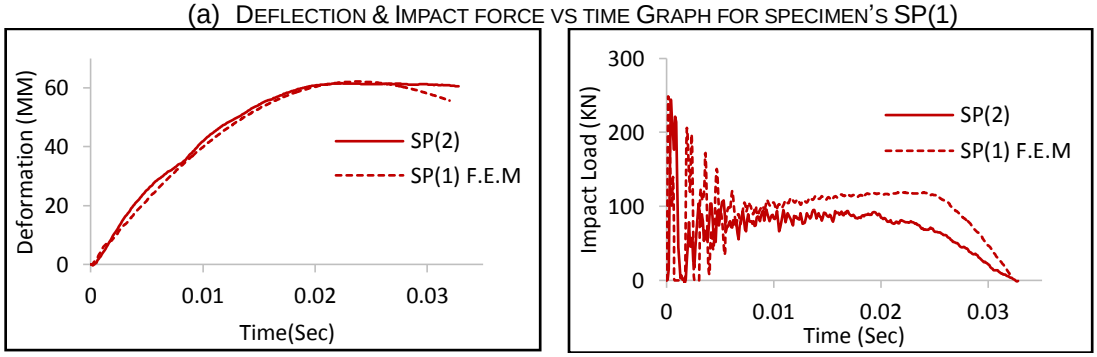

(b) DEFLECTION & IMPACT FORCE VS TIME GRAPH FOR SPECIMEN'S SP(2)

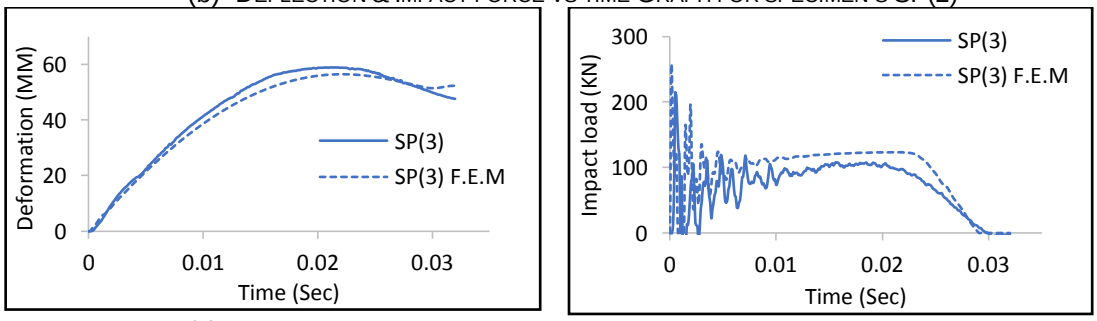

(c) DEFLECTION & IMPACT FORCE VS TIME GRAPH FOR SPECIMEN'S SP(3)

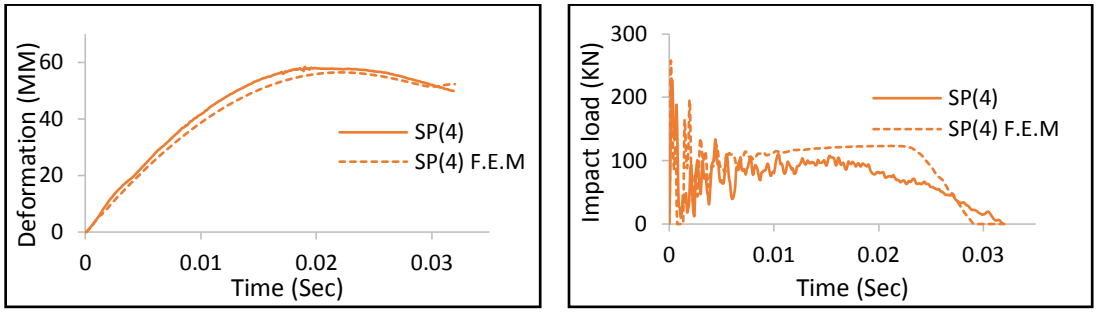

(d) DEFLECTION & IMPACT FORCE VS TIME GRAPH FOR SPECIMEN'S SP(4)

***FIG. 16** COMPARISON BETWEEN THE F.E.M AND TESTED RESULTS FOR SPECIMEN'S SP(1 TO 4)*

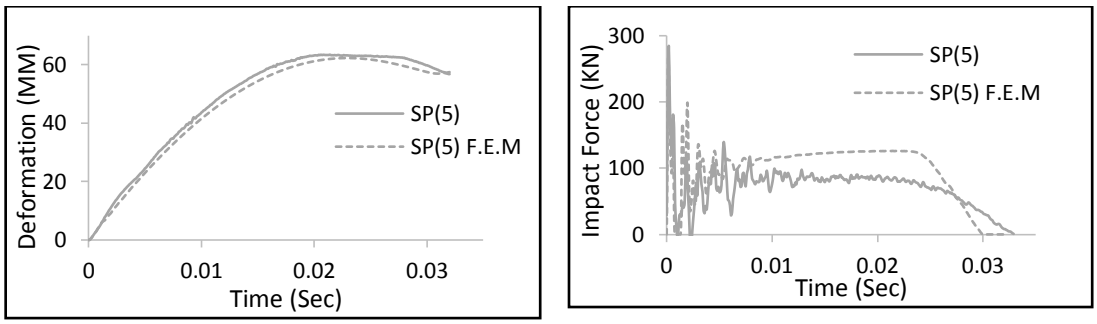

(a) DEFLECTION & IMPACT FORCE VS TIME GRAPH FOR SPECIMEN'S SP(5)

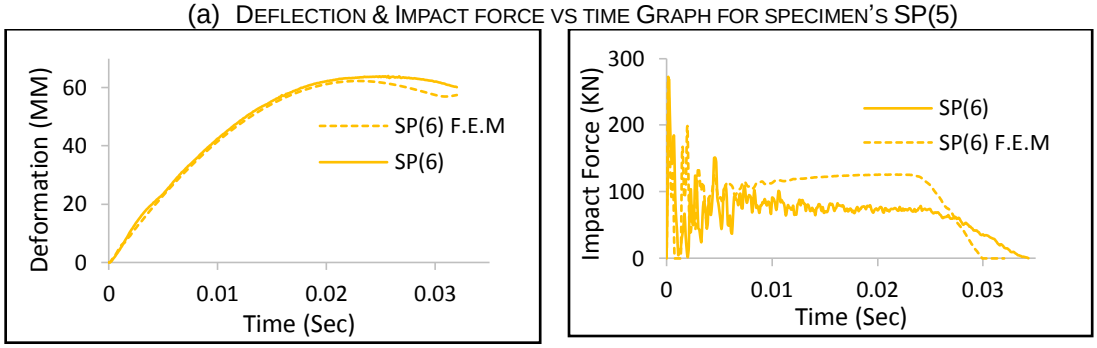

(b) DEFLECTION & IMPACT FORCE VS TIME GRAPH FOR SPECIMEN'S SP(6)

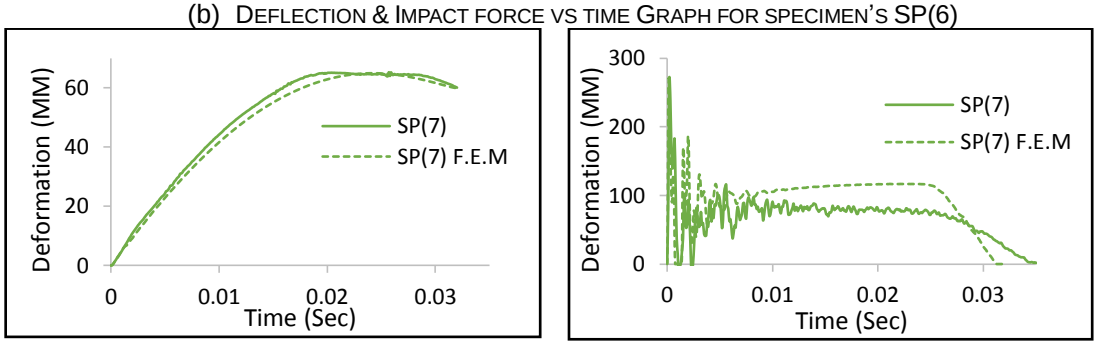

(c) DEFLECTION & IMPACT FORCE VS TIME GRAPH FOR SPECIMEN'S SP(7)

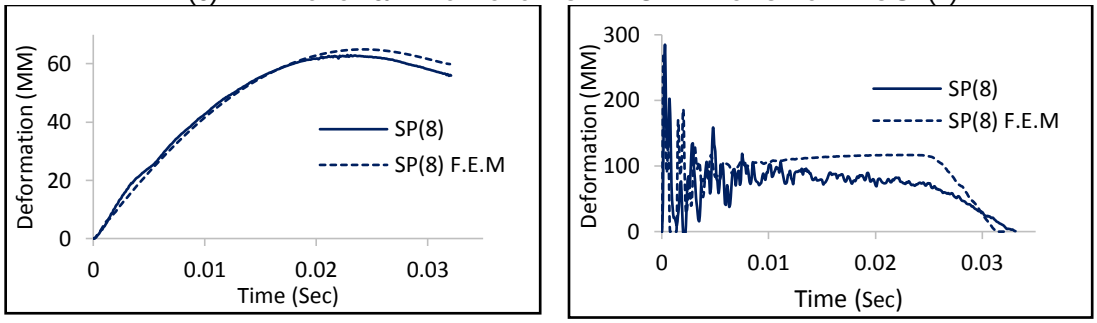

(d) DEFLECTION & IMPACT FORCE VS TIME GRAPH FOR SPECIMEN'S SP(8)

***FIG. 17** COMPARISON BETWEEN THE F.E.M AND TESTED RESULTS FOR SPECIMEN'S SP(5 TO 8)*

5 CONCLUSIONS

An experimental and numerical investigation on the performance of circular CFST members under lateral impact loading filled with different types of concrete is presented in this study. Based on the observations and analytical results, we can conclude that:

(a) Seam welded tube specimens have an almost equivalent lateral impact resistance as the seamless tube counterparts. Nearly, the same maximum dynamic displacement ($u_{mm,e}$), peak ofimpact load ($P_{k,e}$), and total energy (W) were recorded for the seamwelded and seamless tube.
(b) The typical Failure mode of all specimens were characterized by V-shape pattern at the impacted area, where the core concrete was crushed and cracked at the mid-span section and probably fractured near the mid-span and along the flat part.
(c) $P_{k,e}$, $P_{s,e}$, $u_{mm,e,}$ and W of polypropylene concrete specimens were lower than those of all other types of concrete specimens. While the maximum recovery energy $W_{Recovery}$ was recorded for the polypropylene concrete specimens.
(d) The $P_{k,e}$, $P_{s,e}$, $u_{mm,e}$, and W of high strength concrete specimens were nearly the same or slightly higher than those of normal concrete, which mean that, no benefit was gained form increasing the concrete strength. On the other hand, it may have triggered brittle failure for the concrete core.
(e) The deformations for steel fiber concrete, normal concrete, and high strength concrete specimens were nearly in the same values, however, the steel fiber concrete specimens displayed ductile behavior with less concrete cracks.

REFERENCES

[1]. A. Seminar, "Concrete Filled Steel Tubes—A Comparison of International Codes and Practices," Innsbruck, September. Google Scholar, 1997.

[2]. N. E. Shanmugam and B. Lakshmi, "State of the art report on steel–concrete composite columns," Journal of constructional steel research, vol. 57, no. 10, pp. 1041-1080, 2001.

[3]. L.-H. Han, G.-H. Yao, and Z. Tao, "Performance of concrete-filled thin-walled steel tubes under pure torsion," Thin-Walled Structures, vol. 45, no. 1, pp. 24-36, 2007.

[4]. U. Starossek, N. Falah, and T. Lohning, "Numerical analyses of the force transfer in concrete-filled steel tube columns," Structural engineering and mechanics: An international journal, vol. 35, no. 2, pp. 241-256, 2010.

[5]. D. Lam and K. Wong, "Axial capacity of concrete filled stainless steel columns," in Structures Congress 2005: Metropolis and Beyond, 2005, pp. 1-11.

[6]. J.-Y. Kang, E.-S. Choi, W.-J. Chin, and J.-W. Lee, "Flexural behavior of concrete-filled steel tube members and its application," Steel Structures, vol. 7, no. 4, pp. 319-324, 2007.

[7]. S.-F. Jiang, Z.-Q. Wu, and D.-S. Niu, "Experimental study on fire-exposed rectangular concrete-filled steel tubular (CFST) columns subjected to bi-axial force and bending," Advances in Structural Engineering, vol. 13, no. 4, pp. 551-560, 2010.

[8]. H. Sharma, S. Hurlebaus, and P. Gardoni, "Performance-based response evaluation of reinforced concrete columns subject to vehicle impact," International Journal of Impact Engineering, vol. 43, pp. 52-62, 2012.

[9]. B. EN, "1-7 Eurocode I: actions on structures-Part 1-7. general actions—accidental actions [S]," Brussels: European Committee for Standardization, vol. 2006, pp. 53-55, 1991.

[10]. Y.-F. Yang, Z.-C. Zhang, and F. Fu, "Experimental and numerical study on square RACFST members under lateral impact loading," Journal of Constructional Steel Research, vol. 111, pp. 43-56, 2015.

[11]. M. R. Bambach, H. Jama, X. L. Zhao, and R. Grzebieta, "Hollow and concrete filled steel hollow sections under transverse impact loads," Engineering structures, vol. 30, no. 10, pp. 2859-2870, 2008.

[12]. A. Al-Husainy, "Impact response of recycled aggregate concrete filled steel tube columns strengthened with CFRP," University of Liverpool, 2017.

[13]. A.-Z. Zhu, W. Xu, K. Gao, H.-B. Ge, and J.-H. Zhu, "Lateral impact response of rectangular hollow and partially concrete-filled steel tubular columns," Thin-Walled Structures, vol. 130, pp. 114-131, 2018.

[14]. B. En, "197-1: 2011," Cement, Composition, Specifications and Conformity Criteria for Common Cements. London, England: British Standard Institution (BSI), 2011.

[15]. A. No, "Specification for aggregates from natural sources for concrete," ed: BS, 1992.

[16]. U. m. Abaqus and S. U. s. Manual, "Hibbitt, Karlsson, and Sorensen," Inc V5, vol. 8, 2005.

[17]. L.-H. Han, X.-L. Zhao, and Z. Tao, "Tests and mechanics model for concrete-filled SHS stub columns, columns and beam-columns," Steel and Composite Structures, vol. 1, no. 1, pp. 51-74, 2001.

[18]. N. Jones, Structural impact. Cambridge university press, 2011.

[19]. W. Abramowicz and N. Jones, "Dynamic axial crushing of square tubes," International Journal of Impact Engineering, vol. 2, no. 2, pp. 179-208, 1984.

[20]. Z. Tao, Z.-B. Wang, and Q. Yu, "Finite element modelling of concrete-filled steel stub columns under axial compression," Journal of constructional steel research, vol. 89, pp. 121-131, 2013.

[21]. L.-H. Han, G.-H. Yao, and X.-L. Zhao, "Tests and calculations for hollow structural steel (HSS) stub columns filled with self-consolidating concrete (SCC)," Journal of Constructional Steel Research, vol. 61, pp. 1241-1269, 09/01 2005, doi: 10.1016/j.jcsr.2005.01.004.

[22]. D. Carreira and K.-H. Chu, "Stress-strain relationship for plain concrete in compression," Journal of the American Concrete Institute, vol. 82, pp. 797-804, 11/01 1985.

[23]. L. Oliveira Júnior et al., "Stress-strain curves for steel fiber-reinforced concrete in compression," Matéria (Rio de Janeiro), vol. 15, pp. 260-266, 01/01 2010, doi: 10.1590/S1517-70762010000200025.

[24]. A. Committee, "Building code requirements for structural concrete:(ACI 318-02) and commentary (ACI 318R-02)," 2002: American Concrete Institute.

[25]. M. Yousuf, B. Uy, Z. Tao, A. Remennikov, and J. R. Liew, "Impact behaviour of pre-compressed hollow and concrete filled mild and stainless steel columns," Journal of Constructional Steel Research, vol. 96, pp. 54-68, 2014.

[26]. G. Mays, P. D. Smith, and P. D. Smith, Blast effects on buildings: Design of buildings to optimize resistance to blast loading. Thomas Telford, 1995.

[27]. P. Baltay and A. Gjelsvik, "Coefficient of friction for steel on concrete at high normal stress," Journal of Materials in Civil Engineering, vol. 2, no. 1, pp. 46-49, 1990.